JAAS

ROYAL SOCIETY OF CHEMISTRY

PAPER

View Article Online
View Journal

Check for updates

Cite this: DOI: 10.1039/d2ja00132b

ANN-LIBS analysis of mixture plasmas: detection of xenon†

Homa Saeidfirozeh, ‡*[a] Ashwin Kumar Myakalwar, ‡[b] Petr Kubelík,‡[ac] Amirhossein Ghaderi, ‡[d] Vojtěch Laitl, [ae] Lukáš Petera,[a] Paul B. Rimmer,[f] Oliver Shorttle,[gh] Alan N. Heays,[a] Anna Křivková,[ai] Miroslav Krůs,[j] Svatopluk Civiš,[a] Jorge Yáñez, *[b] Erik Képeš, [kl] Pavel Pořízka[kl] and Martin Ferus [a]

Received 19th April 2022
Accepted 1st July 2022

DOI: 10.1039/d2ja00132b

rsc.li/jaas

We developed an artificial neural network method for characterising crucial physical plasma parameters (*i.e.*, temperature, electron density, and abundance ratios of ionisation states) in a fast and precise manner that mitigates common issues arising in evaluation of laser-induced breakdown spectra. The neural network was trained on a set of laser-induced breakdown spectra of xenon, a particularly physically and geochemically intriguing noble gas. The artificial neural network results were subsequently compared to a standard local thermodynamic equilibrium model. Speciation analysis of Xe was performed in a model atmosphere, mimicking gaseous systems relevant for tracing noble gases in geochemistry. The results demonstrate a comprehensive method for geochemical analyses, particularly a new concept of Xe detection in geochemical systems with an order-of-magnitude speed enhancement and requiring minimal input information. The method can be used for determination of Xe plasma physical parameters in industrial as well as scientific applications.

Introduction

Noble gases are a central archive of planetary processes in the geo- and planetary-sciences. Their inert nature and quantity of isotopes provide a clear fingerprint for passive tracing of important volatile species such as CO_2 and H_2O, that are crucial to planetary climate and habitability, and of all the major volatile loss and gain processes that a celestial body experiences over its existence.[1,2] The abundances of noble gases are used as key information when identifying parent bodies of meteorites, thus providing an insight to the history of the whole Solar System.[3] Xe and its nine isotopes have long presented a wealth of information, and generated conundrums in equal measure, on the loss and gain of the atmospheres of Earth and Mars.[4] In particular, it is the strong mass-dependent fractionation of terrestrial and Martian Xe, higher than that of the lighter isotopes of Kr, that presents a puzzle.[5,6] One feature of Xe that stands out, and perhaps explains its significant isotopic fractionation, is its low ionisation threshold, which is lower than that of all other noble gases and than hydrogen.[5] In this context, it will be important in the future to investigate Xe physics in meteor impact plasma and lightning in planetary atmospheres, which may have contributed to Xe's ionization and subsequent distinct loss history compared with the other noble gases. Preferential Xe atmospheric depletion is driven by charge-transfer processes, which strengthens the importance of understanding such phenomena at the atomic level. Research into the trace inert gas detection is also largely driven by the industrial and environmental sectors with the detection of He, Ar, and Xe.[7–11]

[a]J. Heyrovský Institute of Physical Chemistry, Czech Academy of Sciences, Dolejškova 3, CZ 182 23 Prague 8, Czech Republic. E-mail: homa.saeidfirouzeh@jh-inst.cas.cz
[b]Laboratorio de Trazas Elementales y Especiación, Departamento de Química Analítica e Inorgánica, Facultad de Ciencias Químicas, Universidad de Concepción, Concepción, Chile. E-mail: jyanez@udec.cl
[c]Department of Radiation and Chemical Physics, Institute of Physics, Academy of Sciences of the Czech Republic, Na Slovance 1999/2, CZ182 21 Prague 8, Czech Republic
[d]Centre for Vision Research, York University, 4700 Keele St, Toronto, ON M3J 1P3, Canada
[e]University of Chemistry and Technology Prague, Faculty of Chemical Engineering, Technická 5, CZ166 28 Prague 6 Dejvice, Czech Republic
[f]Cavendish Astrophysics, University of Cambridge, JJ Thomson Ave, Cambridge, CB3 OHE, UK
[g]Institute of Astronomy, University of Cambridge, CB3 0HA, UK
[h]Department of Earth Sciences, University of Cambridge, CB2 3EQ, UK
[i]Czech Technical University in Prague, Faculty of Nuclear Sciences and Physical Engineering, Brehová 78/7, 115 19 Prague 1, Czech Republic
[j]Institute of Plasma Physics, Czech Academy of Sciences, Za Slovankou 1782/3, 182 00 Prague 8, Czech Republic
[k]Central European Institute of Technology, Brno University of Technology, Purkyňova 656/123, CZ-61200, Brno, Czech Republic
[l]Brno University of Technology, Faculty of Mechanical Engineering, Institute of Physical Engineering, Technická 2, CZ-61669, Brno, Czech Republic

† Electronic supplementary information (ESI) available. See https://doi.org/10.1039/d2ja00132b

‡ These authors contributed equally to this work.

The quantitative determination of noble gases can be achieved by using laser-based spectroscopies such as laser absorption spectroscopy (LAS)[12] and laser-induced breakdown spectroscopy (LIBS). The LAS technique is very sensitive and advantageous in terms of limit of detection (LOD) compared to LIBS, however, the experimental procedure is tedious and time-consuming. LIBS is valuable in the scenarios of online *in situ* monitoring of noble gas contents and also for determining the properties of plasma. The established quantitative analyses using LIBS comprise (i) calibration (univariate and multivariate), and (ii) calibration-free methods. Regarding plasma diagnostics, one can determine the properties of plasma using Saha–Boltzmann equations[13] and direct measurements using the Langmuir probe.[14] The chosen method for a given experiment should be robust even with the inclusion of fluctuations in the spectral data and noise.

Spectroscopic explorations towards noble gases are challenging due to their high ionisation energies. With increasing laser energy, the continuum background also increases in the recorded laser-induced break-down spectra. Thus, the optimization of experimental conditions represents a very complicated task, frequently addressed by well-designed *ad hoc* campaigns. For instance, Eseller *et al.* have concluded that non-gated detection exhibits up to four times better performance by using a simple calibration methodology[9] and further introduced the quantitative detection of He in H_2 gas mixtures.[10] Recently, Burger *et al.* demonstrated trace Xe detection in He mixtures for monitoring nuclear fuel failure.[11]

The main objective of this work is to introduce a novel and potentially routine method based on the Artificial Neural Network (ANN) for the estimation of physical parameters and speciation analysis of noble gases-containing plasma relevant in geochemistry and meteoritics. So far, the determination of plasma parameters such as plasma temperature and electron number density using joint plasma LTE model and ANN models has only been reported for solid state materials such as titanium[15] or Ni–Cu alloys.[16] Our method is suitable for remote sensing (such as meteor plasma spectroscopy in planetary atmospheres), probing techniques for planetary landers and rovers as well as for laboratory purposes. This paper is organised as follows: first, a concise summary of the classical LIBS protocol is presented. Then, we present the proposed model and numerical ANN approach and after that, the experimental setup, materials, and methods used for data acquisition are described. Finally, we discuss the results achieved and offer conclusions and outlines for further research.

Theory and computation

All recorded data were evaluated by several analytical approaches and models. First, the ANN was trained on the data set of pure Xe spectral lines. For the training part, line profiles were used as an input and physical plasma parameter estimated from the corresponding Xe spectra by classical approaches as output. Namely, the temperature was calculated by the classical Boltzmann plot method of Xe II spectral intensities. The electron number density calculated from the emission line's broadening using Start broadening parameters taken from ref. 17. Alternatively, electron number density was also estimated from the ratios of emission lines of different Xe ionisation states calculated by Saha ionization equation. Then, we used a blind data set, never employed during the training step, without having any out-put projected on the model and we predicted plasma parameters. Subsequently, the results were verified numerically by LTE simulations.

Local thermodynamic equilibrium

The classical LIBS protocol[18–21] is a powerful tool for describing the physical state of optically thin LIBS plasma that satisfy local thermodynamic equilibrium (LTE) conditions throughout the temporal and spatial observation window.[22,23] The observed intensity, I_{ij}, of a particular atomic emission line corresponding to the transition $i \rightarrow j$ is therein expressed as[24]

$$I_{ij} = FN_{\mathrm{S}}\frac{A_{ij}g_i h\nu_{ij}}{4\pi Q_{\mathrm{S}}(T)}\exp\left(-\frac{E_i}{k_{\mathrm{B}}T}\right). \tag{1}$$

Here, F is an experimental factor related to the apparatus optical collection efficiency and characteristic length of the plasma, N_{S} is the abundance of species S in a particular ionisation and excitation state, A_{ij} is the Einstein A coefficient, g_i is the upper-state degeneracy, h is the Planck constant, and ν_{ij} is the transition frequency. T is the plasma temperature, understood as a limit of the free electron translational temperature, T_{e}, and k_{B} is the Boltzmann constant. The separate partition function of the neutral or ionic species can be expressed as follows:

$$Q_{\mathrm{S}}(T) = \sum_i g_i \exp\left(-\frac{E_i}{k_{\mathrm{B}}T}\right). \tag{2}$$

Under the assumption of LTE, eqn (2) and Boltzmann statistics fully describe the state of a LIBS plasma and its spectroscopic properties. When the number densities of different charged states are factored out from the Boltzmann law, the Saha ionisation equation can be expressed as

$$\frac{N^{Z+1}N_{\mathrm{e}}}{N^{Z}} = \frac{(2\pi m_{\mathrm{e}}k_{\mathrm{B}}T_{\mathrm{e}})^{\frac{3}{2}}}{h^3}\frac{2Q^{Z+1}(T)}{Q^{Z}(T)}\exp\left(-\frac{E_{\infty}{}^{Z}-\Delta E}{k_{\mathrm{B}}T_{\mathrm{e}}}\right). \tag{3}$$

N_{e} is the electron number density, m_{e} the electron rest mass, and $E_{\infty}Z$ is the ionisation energy of the Zth ionisation state corrected by the energy ΔE. The latter term describes interactions inside the plasma and in a collision-determined LTE plasma equilibrated at the temperature, such that $T = T_{\mathrm{e}}$, it may be reasonably neglected.

The electron number density of the plasma is related to the Stark collisional broadening of spectral lines. The half-width γ of a Stark-broadened spectral line can be calculated by the following expression:

$$\gamma = 2\Omega\left(\frac{N_{\mathrm{e}}}{N_{\mathrm{e}}^{*}}\right) + \frac{7\Omega A}{2}\left(\frac{N_{\mathrm{e}}}{N_{\mathrm{e}}^{*}}\right)^{\frac{5}{4}}\left(1-\frac{3}{4}N_{\mathrm{D}}^{-\frac{1}{3}}\right), \tag{4}$$

where Ω is the electron-impact parameter,[17] A is the ion broadening parameter, N_e^* is a reference value obtained from a database,[25] and N_D is the number of particles within the Debye sphere.

Under the experimental conditions considered here, ion broadening parameters are typically an order-of-magnitude less than Ω. Thus, the second term in eqn (4) attributable to ion broadening can be neglected, giving an approximation

$$\gamma \simeq 2\Omega\left(\frac{N_e}{N_e^*}\right) \tag{5}$$

With this simplification, eqn (5) is just attributed to the broadening due to electron collisions, allowing us to calculate the electron number density from the Stark broadening of well-defined spectral lines adopting a Lorentzian line shape function.[25–30]

Then, the validity of the LTE approximation can be expressed by the McWhirter criterion:[23]

$$N_e \geq 1.6 \times 10^{12}\ \left(\mathrm{cm}^{-3}\ \ \mathrm{eV}^{-7/2}\right) \times T^{\frac{1}{2}} \Delta E^3 \tag{6}$$

where ΔE (eV) is the largest energy gap between two distinct energy levels. The minimum electron number density of a warm laser-induced plasma in LTE is then of the order of 10^{15} cm^{-3} for large laser sparks or 10^{16} cm^{-3} for plasma's yielded by smaller laboratory laser equipment (see the *Experimental* section).

Artificial neural network analysis

An Artificial Neural Network is inspired by network of neurons in animal brains. It is a computational model designed to simulate the way the animal brain visualizes and processes information.[31] Generally, ANNs are constructed from several processing units and connections between these units (synaptic weights). These networks use several computational units arranged in different layers. There are many different types of these networks. One of the most useful and popular types of ANNs are multi-layer perceptron (MLP) networks constructed by one input layer, one output layer, and at least one computational intermediate layer between them (see Fig. 1). These intermediate layers are known as hidden layers.[32] The MLPs need a supervised learning algorithm to find the best fit between their calculated output and target. The algorithm consists of three steps: training, validation, and testing. In the training step, the inputs and targets of training datasets are presented to the network and weights and biases are adjusted between all perceptrons to find the best fit between the network's outputs and desired outputs from the data provided. In the validation step, the validation data-set is used to evaluate the model obtained after the training step. Validation is used to optimise the model's architecture. Finally, in the testing step, the trained model (configured with validation set) is evaluated using the test data-set, which was not present to the model during the training or validation. Generally, the division of the data comprises 65% for training, 20% for validation, and 15% for testing. The ANN's performance can be evaluated using countless metrics. Since the prediction of the plasma temperature is a regression problem, here we use the mean square error (MSE) and correlation coefficient (R^2) metrics. The network was trained using several variations of gradient descent (GD) with back-propagation (BP). In summary, the output set of MLP is compared with the desired output set to find the error function of the network, e, as follows:[33]

$$e = \frac{1}{2}\sum_{i=1}^{p}\left(o_i - t_i\right)^2, \tag{7}$$

where p stands for the number of data points in training set, o_i is the output of the network, and t_i is desired output of the network. This error function is propagated backwards through in the network to modify the synaptic weights and biases. The modified synaptic weights should then minimise e by an iterative gradient descent approach:

$$\Delta W = -\Gamma \frac{\partial e}{\partial w_i}, \tag{8}$$

where w_i stands for one synaptic weights and Γ is the learning rate. Several modified versions of the GD algorithm have been proposed to overcome the fitting performance issues. More details about the used GD algorithm can be found in the supplementary part.

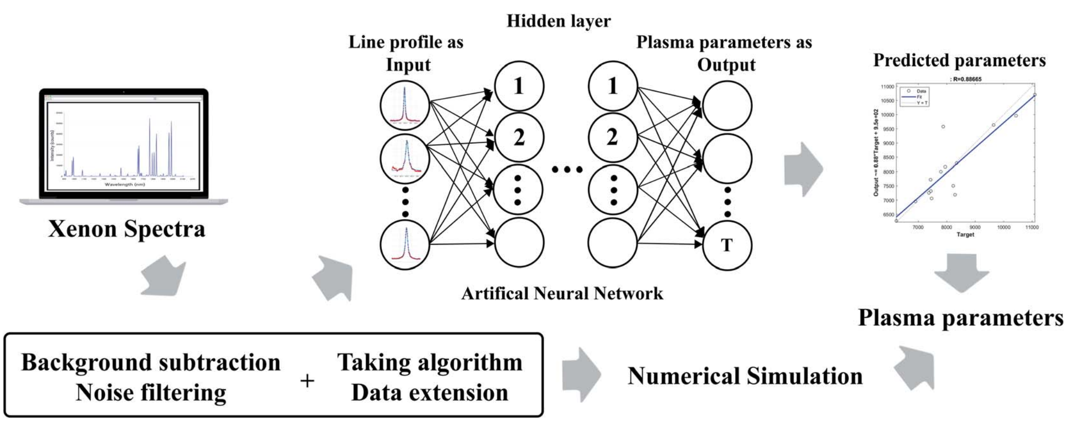

Fig. 1 Schematic of the artificial neural network (top) and numerical simulation approaches (bottom) for the calculation of plasma parameters.

Numerical simulation

A complete analysis of Xe gas emission spectra is challenging due to a number of instrumental and experimental limitations. For instance, the effective wavelength range of UV-Vis spectrometers conventionally used does not allow the detection of most emission lines of neutral Xe and we must therefore rely on analysing its ionised states. However, high laser energies and high pressure of the buffer gas need to be applied in such cases due to remarkable ionisation energies of rare gas atoms.[34] This in turn introduces increased continuum background and noise levels, which corrupts the precision of routinely used Boltzmann plot or related linearisation methods. Another computational approach was hence needed for this study.

Our computation comprised numerical optimisation of intensive plasma properties (*i.e.*, T, N_e, and elemental abundances) onto line intensity profiles and integral values obtained by an experiment (see Fig. 2). First, electron density values were guessed by fitting the detector instrumental function enhanced by Stark broadening eqn (5) onto well-defined spectral line profiles. An initial estimate of remaining plasma parameters was then provided by the diagrammatic solution to eqn (1) estimating the unknown temperature and number density of a given species *via* the Boltzmann plot[19] method. The set of guessed values served as an initial estimate for global line intensity optimisation, which resulted in estimating plasma temperature, electron density, and abundances values relevant to the whole spectral sample. Finally, a synthetic spectrum governed by the resultant properties was depicted and compared to the experiment. If necessary, numerical results were employed as an initial estimate for another iteration until a reasonable (*i.e.*, $R^2 > 0.98$) agreement was reached. All details of this procedure and developed model can be found in the supplementary part.

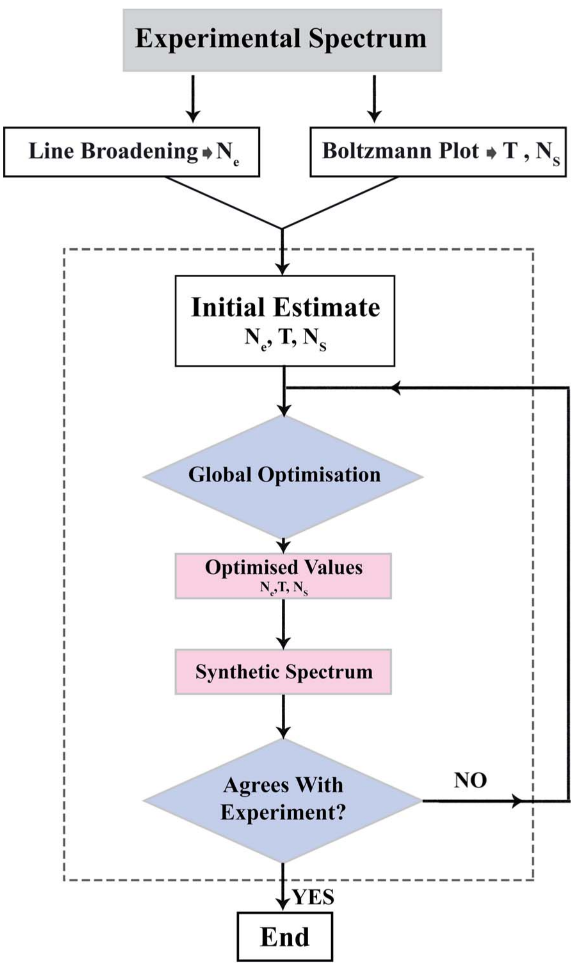

Fig. 2 Block diagram for the simulation of xenon gas spectra.

Experimental

Apparatus

Gas phase laser-induced dielectric breakdown emission spectroscopy was performed using two different laser systems. Pure Xe laser sparks were generated by a table top Nd:YAG laser (see Fig. S1†). Then, the Prague Asterix Laser System (PALS) facility, introduced by Jungwirth *et al.*[35] and briefly described below, was employed for igniting high energy-density plasma in the gaseous mixtures selected. Certified gas samples, *i.e.*, 5.0 Linde Gas Xe, 3.6 Messer N_2, 3.0 Linde Gas CO, and 3.0 Linde Gas CH_4 were used in the experiment. Water vapour was supplied with freshly distilled water which was let freely vaporise from a closed round flask connected to the gas collecting cell with a PVA pipe. The total pressure was controlled with a pressure gauge to reach the desired partial pressures.

In both setups, the radiation emitted by the gas phase laser induced breakdown plasma was analysed by high resolution ESA 4000 Echelle spectrograph (LLA Instruments GmbH, Germany). The effective wavelength range of the detector reaches from 200 to 780 nm with spectral resolution ranging from 0.005 nm (200 nm) to 0.019 nm (780 nm) and the aperture of 1 : 10. Emission from the plasma was coupled to the spectrometer through a fibreoptic cable without additional light-collecting optics employed. The time delay between initiation and observation of the laser-induced plasma was controlled with the ESAWIN software version 14.3.0.

Nd:YAG laser

Laboratory LIBS system (Fig. S1 in the ESI†) comprises a first harmonic pulsed Nd:YAG laser operating with 10 Hz repetition rate, delivering maximum pulse energy of 850 mJ at the fluence of 15 J cm^{-2}. The laser pulse is focused in the centre of a cylindrical glass sample cell equipped with three windows by using a plano-convex lens of 15 mm diameter and a focal length of 105 mm. A vacuum pump and pressure gauge (Pfeiffer Vacuum Austria GmbH) regulated the flow of gases and cell pressure.

PALS laser

PALS (Prague Asterix Laser System[35]) terawatt-class facility is operated on a highly exergonic $^2P_{1/2} \rightarrow {}^2P_{3/2}$ de-excitation of iodine atoms generated by homolytic fission of perfluoroisopropyl iodide, C_3F_7I. The radiation intensity generated by each 100 to 600 J laser pulse is of the order of magnitude 10^{13} W m^{-2} with the fluence of 30 J cm^{-2} and the system delivers one pulse approximately every 30 minutes. The main difference between the PALS LIBS system and the Nd:YAG setup is the density of energy per pulse, increased nearly by 3 orders of magnitude, and resulting in enhanced degrees of atomic excitation and ionisation. PALS laser sparks are hence an ideal example of complex systems enabling more significant ionisation of noble gases thanks to the high energy density delivered. While higher ionisation degrees are advantageous for our analyses, the corresponding laser spark spectra are, on the other hand, more complex to evaluate due to the issues mentioned above. This in turn makes PALS laser sparks a matching case study for testing the viability and robustness of novel neural network algorithm.

Data acquisition and initial conditions

About 275 LIBS spectra, collected across both laser systems, were recorded in wavelength range between 200 to 750 nm. In order to investigate the time evolution of the pure gas systems in Nd:YAG laser sparks, the spectra were measured for different t gate delays at 10 500 ns, and then from 1000 to 3000 ns with a time-step of 1000 ns. High-pressure (120, 709 Torr) and low-pressure (39, 72 Torr) Nd:YAG laser sparks were examined for the determination plasma parameters and abundances.

PALS laser sparks were delivered to approximately equimolar mixtures of CO, CH_4, and N_2 filled with a small addition of water vapor. This composition was chosen in order to elaborate our previous investigations on a mimicked early Earth or Titan atmosphere,[37] this time diluted with an inert gas. Furthermore, the choice of model mixtures coincides with recent studies (Mahajan *et al.*[38] and references therein) tracing Xe and other noble gases in meteorites by pyrolytic analyses. Therefore, it proves the concept of detecting noble gases in geochemically relevant systems and suggests a possible way of employing our protocol in related settings of laboratory astrophysics.[39–42]

The mixtures prepared were diluted with xenon (1 : 2) up to two different pressures, as indicated in Table 1. Both mixtures were scanned at gate delay times of 100, 2000, 3000, 4500, and 6500 ns. The criteria for selecting these delay times are purely experimental to find the optimal signal/noise ratio. Moreover, the latter gate delay times extended our observation to the afterglow period of the large laser sparks ignited. After each experiment, gaseous products were carefully washed out with an excess of Xe and the sample cell was refilled using pressure gauges.

Table 1 Identification of mixture samples comprising their net pressure, molar composition, and the pressure of diluting Xe

	mol%					
Sample no.	H_2O	CO	CH_4	N_2	p (Torr)	p_{Xe} (Torr)
1	1.8	32.8	32.5	32.9	15	30
2	1.8	32.9	32.4	32.9	10	20

Software and computing

Most of the data analysis was performed using the MATLAB neural network toolbox.[43,44] The code is developed based on local thermodynamic equilibrium theory. Spectral line selection, electron and heavy particle number density fitting, and numerical simulations of emission spectra were automated by using in-house programmed scripts (custom-code which programmed by the Spectroscopy research team, J. Heyrovský Institute of Physical Chemistry of the Czech Academy of Sciences). The latter were covered by PYTHON modules NUMPY and SCIPY. The choice of modules, namely SCIPY, helps to overcome the computational time costs resulting from the non-typed character of PYTHON language. According to the procedure of Gornushkin *et al.*,[45] the sensitivity of our procedure to noise level, line overlap, and self-absorption related phenomena was tested before simulation. Self-absorption of investigated spectral lines is corrected by simpler means of self-absorption coefficients[46–49](see the ESI† part for details).

Results and discussion

In the present work, the ANN approach along with a comprehensive experimental analysis of xenon plasma exposed to the laser spark was reported. To verify our experimental observations and computations, an LTE model was used for simulating the plasma systems under experimental conditions. Plasma temperature was recorded in the range of 14 000–26 000 K, and electron densities of 10^{16}–10^{17} cm^{-3}. While the plasma temperatures are rather large, they agree with both the McWhirter criterion and the assumptions mentioned above. If a high ionisation potential of rare gas atoms is to be crossed, it is necessary that the plasma should be equilibrated to high temperatures, even to those repeatedly observed in our data.

Our ANN analysis of aforementioned LIBS data confirms the stability and robustness the proposed approach. The details are provided in the following sections, specifically describing the amelioration of obstacles arising from high ionization energy of Xe, range of the spectrometer.

Spectral lines selection and plasma diagnostics

A typical experimental LIBS spectrum of pure gas-phase Xe is shown in Fig. 3. The recorded Xe II emission lines are summarised in Table 2. From the experimental point of view, Xe spectroscopy performed by standard Echelle UV-Vis apparatus is harder due to the effective operational wavelength range of conventional high resolution spectrometers being within 200–800 nm, which is problematic since the most intense lines of Xe I appear in the range of 800-850 nm.[11] Our comparison of numerical simulations to experimental data identifies the only Xe I line at 476.123 nm. The lines related to Xe III state were not assigned either, since no theoretical data of Xe III lines appear in NIST database[36] or other resource.[50–53] Unfortunately, missing evidence of other ionisation states than Xe II corrupts the conventional LIBS protocol and prevents it from robust usage. However, this can be overcome by using the ANN approach to analyse solely the Xe II emission lines of good signal-to-noise

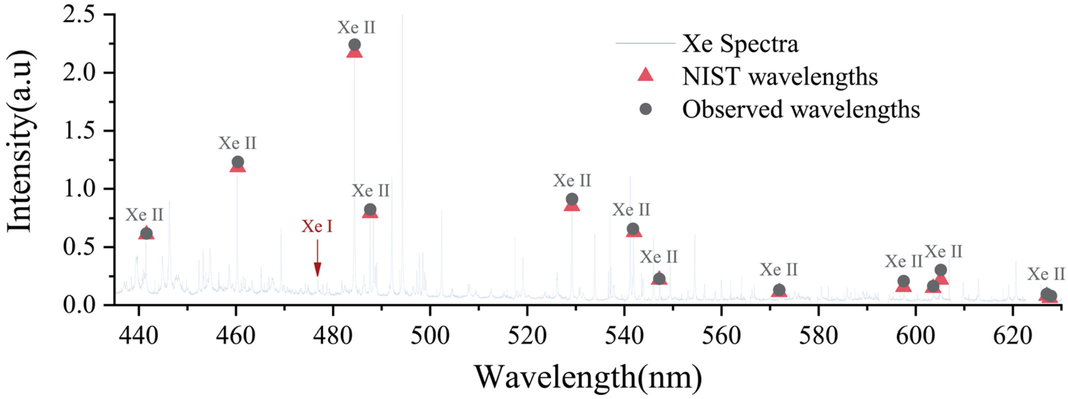

Fig. 3 Example of the experimental Xe spectra. Triangle and circle symbols, respectively, represent the assigned (ref. 36) and observed wavelengths for Xe II. Moreover, the red arrow shows the single Xe I line observed.

Table 2 The reference data of Xe II emission lines utilised in this work

Species	Wavelength (nm)	Upper level energy (cm^{-1})	A_{ij} (10^8 s^{-1})	g_i	Ref
Xe II	441.482	132 207.76	1.00	6	54
Xe II	460.304	116 783.09	0.82	4	54
Xe II	484.432	113 705.40	1.10	8	54
Xe II	487.649	130 063.96	0.63	8	54
Xe II	529.221	111 958.89	0.89	6	54
Xe II	541.914	113 512.36	0.62	6	54
Xe II	547.261	113 705.40	0.09	8	54
Xe II	571.960	113 512.36	0.06	6	54
Xe II	597.642	111 792.17	0.28	4	54
Xe II	603.619	111 958.89	0.07	6	54
Xe II	605.115	111 958.89	0.17	6	54
Xe II	627.086	128 867.20	0.18	6	54
Xe II	627.754	111 958.89	0.03	6	54

ratio acquisitions. Details of the ANN procedure are summarised below.

Plasma diagnostics using ANN

For real-time plasma diagnostics, ANN was implemented and trained with pure Xe LIBS data.

In the ANN approach, only experimental LIBS data were considered. No theoretical parameters or instrumental aspects, such as pressure and gate delay, were taken into account. The pixels describing line emission profiles of listed Xe II in Table 2 were considered as an input to the ANN model and the plasma parameters calculated using LTE model were considered as output. The input data resulted from time-resolved experiments of different gas pressures. The model error was adjusted using validation data and the performance was tested using test data set. We adopted Bayesian regularization (BR) method, which has the best performance in our past findings.[55–58] To understand the efficacy of the different types of GD algorithm, we tested the performance of them, detailed can be found in the supplementary.

In the first step, Xe II lines listed in Table 2 were extracted from the recorded spectra as input, while other parameters such as electron density, composition, and the temperature were utilised as output for the model. To solve the over-fitting problem that usually happens for the smaller size data-sets like ours, a Bayesian regularization modification has been proposed. The results of these algorithms were compared to find the best algorithm for our data-set. The electron density, plasma temperature, and abundance ratios calculated from eqn (1), (3) and (4) were considered as ANN targets and resulting predictions are shown in Fig. 4(a), (b), and (c) respectively. All the pixels within the Lorentzian profile of the Xe II at 484.3 nm were considered for the electron density calculations, while integrated intensities of emission lines of Xe II provided in Table 2 are considered for remaining estimations. As mentioned earlier, all input data were divided into three parts with automatic stratified data division algorithm. The R^2 prediction of all the test data sets superior than 0.9. The root mean square error of prediction (RMSEP) values are less than 4%, and as a result, the error bars are difficult to be differentiated in the figures.

After appropriate training of the ANN with basic physical relations between experimentally measured line intensities and the plasma parameters of pure Xe samples, the ANN can be used for the prediction of the plasma parameter of the unknown samples. To simplify the initial idea about the trapped noble gas in meteorites, xenon gas was examined in presence of a model atmosphere, and the trained ANN was used to predict its plasma parameters. It is clear from the green dots in Fig. 4 that, the ANN is able to predict promising plasma parameters independently of sample composition (*i.e.*, of molar fractions of H_2O, CO, CH_4, N_2, and Xe). This is the proof of concept that we will be able to detect noble gas in such atmospheres. The future idea of this work is to test the developed ANN on the LIBS scanning of stepwise meteorite pyrolysis.[7,59,60] In such applications, ANN can be a very affordable approach which avoids time-consuming LIBS simulations and analyses. Moreover, if certain theoretical values (*e.g.*, transition probabilities of certain species) needed for plasma parameter calculation are lacked, the neural network approach can be used nonetheless. Once the ANN models is prepared, the extraction of plasma parameters from spectral data is possible within a couple of seconds, while

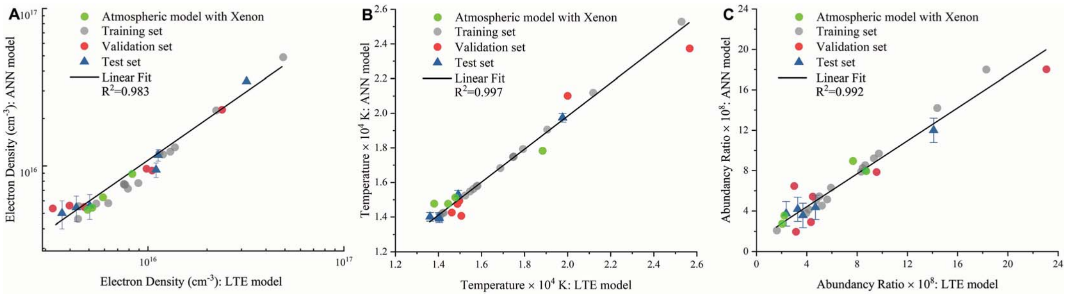

Fig. 4 ANN-predicted *vs.* LTE model-based results for (a) electron number density, (b) temperature, and (c) abundance ratios of xenon states. The regression coefficients are also reported. Gray and red dots mark are related to the training and validation data, respectively. Blue triangles show test data sets results of the pure xenon from the Nd:YAG laser. Light-green dots represent the predicted results for xenon in the model atmosphere irradiated by the PALS laser.

a common desktop PC must devote up to 5 hours to a single simulation below. To our knowledge, such speed and effectiveness in real-time determination of gaseous plasma parameters is first reported in this publication.

Plasma diagnostics using numerical simulation

The performance and results of the above ANN protocol were confirmed by a simpler LTE-based plasma simulation under the same experimental conditions, as outlined in the *Numerical simulation* section. Fig. 5(a) shows the simulated LIBS spectrum of Xe gas in the wavelength range from 523 to 532 nm. The spectrum was simulated for the entire wavelength region, but this specific part was selected because it included all intense atomic and ionic lines. Xe II 529.221 nm emission line was observed with a high signal-to-nose ratio, which is in agreement with experimental observations. The atomic and higher ionic lines are very weak in our experimental conditions, and it is very difficult to distinguish them from the noise level.

Fig. 5(b) shows the time evolution of electron density (red cubes) and plasma temperature (blue points) for a representative series of Nd:YAG measurements (p = 120 Torr). Electron density exponentially decreases with gate delay observation time. This can be ascribed to the exponential decay of plasma spark pressure, as investigated *e.g.*, by Tholin *et al.*[61] Additionally, the linear decrease of plasma temperature can be ascribed to a Newtonian cooling model, addressed in the supplementary part. This model suggests that the general temperature decay should be exponential and should limit to a linear decrease for high temperatures or small temperature differences found. Our findings are in a good agreement with the results of Mal *et al.*[62] Finally, Fig. 5(c) shows the evolution of Xe excited and ionized states abundances expressed as molar fractions against plasma temperature. Abundances of Xe I and Xe II were extracted from synthetic spectra and used to extrapolate the Xe III abundance by eqn (3). Both experimental results and trend fit obtained from the Saha equation converge to the coincidence of ionization states abundances at ≈20 000 K. Since all aforementioned results confirm the neural network predictions, the above ANN protocol appeals as a fast, comprehensive, and precise method for analysing noble gases spectra.

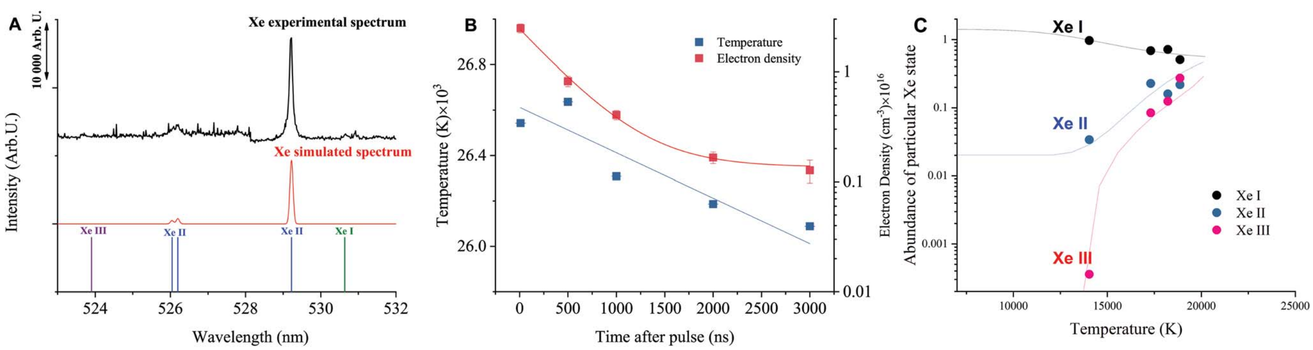

Fig. 5 Example results of numerical simulations. (a) Comparison of Nd:YAG experimental Xe spectra at $p = 120$ Torr and GD = 1500 ns (black line) and simulation results (red line). Green, blue, and purple vertical lines respectively indicate the positions of Xe I, Xe II, and Xe III lines extracted from the NIST database. The leftmost Xe III emission line is marked in its hypothetical position, but to the best knowledge of the authors, no transition probabilities thereof are currently available. The noise level reaches a mean value of 0.015 a.u. with the standard deviation of 10−2. (b) Simulated plasma physical diagnostics for Nd:YAG laser induced plasma of a representative series with total pressure 120 Torr. The red and blue lines show the best exponential and linear fit of simulation data, respectively. (c) State diagram representing the abundance of particular Xe states as a function of temperature at the total pressure of 120 Torr. Solid lines show the simulated fit.

Conclusions

The characterization of LIBS spectra with simple ANN protocols and numerical simulations was performed for xenon, selected for its high geochemical relevancy. Important plasma parameters for LIBS, temperature and electron, are correlated with Xe abundances using an LTE model and a pre-trained network performed similar speciation analyses in gaseous mixtures. Our newly developed and optimised analyses can be performed in seconds and the achieved results are firmly confirmed by an independent numerical simulation. Best-performing algorithms achieve >99% prediction accuracy and >90% correlation with the simulation results. The latter was performed with high precision, with relative uncertainties ≤3%. However, these results have been achieved in order-of-magnitude longer timescales.

The newly developed method has a great application potential in the field of geochemistry and astronomy. In particular, the case study demonstrates the method suitable for the detection of Xe in a gaseous atmosphere relevant to the geochemical environment of terrestrial planets and it is conceptually similar to gas mixtures analysed after pyrolysis of meteorite samples. ANN-LIBS is capable of fast and direct linking the properties of inspected plasma to its elemental analysis. Moreover, our method is very fast, and therefore suitable for real time *in situ* analysis.

Author contributions

HS – conceptualization, resources, supervision, visualization, original draft preparation, review & editing; HS, PK, AHG, AKM, VL, MF – formal analysis, investigation, methodology, software, review & editing, LP, MF – data curation, BPR, OS, AH, AK, JY, EK, PP – writing, review & editing, MF, JY, PP, – funding acquisition.

Conflicts of interest

There are no conflicts to declare.

Acknowledgements

The authors would like to acknowledge the support of this research by grant no. 21-11366S of the CzechScience Foundation and JHI would like to acknowledges ERDF/ESF "Center of Advanced Applied Sciences" (No. CZ.02.1.01/0.0/0.0/16_019/0000778). JY also acknowledges the Chilean National Agency of Research and Development (ANID) Fondecyt 3200371 and project Fondecyt 1191572. PP acknowledges the support by Brno University of Technology under grant no. FSI-S-20-6353. AKM acknowledges the funding from FONDECYT POSTDOC 3200371.

Notes and references

1 B. Marty, K. Altwegg, H. Balsiger, A. Bar-Nun, D. Bekaert, J.-J. Berthelier, A. Bieler, C. Briois, U. Calmonte and M. Combi, *Science*, 2017, **356**, 1069–1072.
2 S. Mukhopadhyay and R. Parai, *Annu. Rev. Earth Planet. Sci.*, 2019, **47**, 389–419.
3 T. Smith, P. Ranjith, H. He and R. Zhu, *Geosciences*, 2020, **10**, 439.
4 R. O. Pepin, *Icarus*, 1991, **92**, 2–79.
5 K. J. Zahnle, M. Gacesa and D. C. Catling, *Geochim. Cosmochim. Acta*, 2019, **244**, 56–85.
6 O. Shorttle, H. Saeidfirozeh, P. B. Rimmer, V. Latil, P. Kubelik, L. Petera and M. Ferus, *Nat. Astron.*, 2022, in preparation.
7 H. McSween Jr and G. Huss, in *Cosmochemistry*, Cambridge University Press, Cambridge, 2 edn, 2022, pp. 400–418.
8 E. McNaghten, A. Parkes, B. Griffiths, A. Whitehouse and S. Palanco, *Spectrochim. Acta B Atom Spectrosc.*, 2009, **64**, 1111–1118.
9 K. E. Eseller, F.-Y. Yueh and J. P. Singh, *Appl. Phys. B*, 2011, **102**, 963–969.
10 K. E. Eseller, F.-Y. Yueh, J. P. Singh and N. Melikechi, *Appl. Opt.*, 2012, **51**, B171–B175.
11 M. Burger, L. Garrett, A. Burak, V. Petrov, A. Manera, P. Sabharwall, X. Sun and I. Jovanovic, *J. Anal. At. Spectrom.*, 2021, **36**, 824–828.
12 P. Jacquet and A. Pailloux, *J. Anal. At. Spectrom.*, 2013, **28**, 1298–1302.
13 H. R. Griem, *Plasma Spectroscopy*, McGraw-Hill. Inc., New York, 1964.
14 B. Doggett and J. G. Lunney, *J. Appl. Phys.*, 2009, **105**, 033306.
15 F. O. Borges, G. H. Cavalcanti, G. C. Gomes, V. Palleschi and A. Mello, *Appl. Phys. B*, 2014, **117**, 437–444.
16 E. D'Andrea, S. Pagnotta, E. Grifoni, S. Legnaioli, G. Lorenzetti, V. Palleschi and B. Lazzerini, *Appl. Phys. B*, 2015, **118**, 353–360.
17 N. Konjević, A. Lesage, J. R. Fuhr and W. L. Wiese, *J. Phys. Chem. Ref. Data*, 2002, **31**, 819–927.
18 M. L. Najarian and R. C. Chinni, *J. Chem. Educ.*, 2013, **90**, 244–247.
19 A. Ciucci, M. Corsi, V. Palleschi, S. Rastelli, A. Salvetti and E. Tognoni, *Appl. Spectrosc.*, 1999, **53**, 960–964.
20 E. Tognoni, G. Cristoforetti, S. Legnaioli, V. Palleschi, A. Salvetti, M. Müller, U. Panne and I. Gornushkin, *Spectrochim. Acta B Atom Spectrosc.*, 2007, **62**, 1287–1302.
21 J. El Haddad, L. Canioni and B. Bousquet, *Spectrochim. Acta B Atom Spectrosc.*, 2014, **101**, 171–182.
22 M. Skočić and S. Bukvić, *Spectrochim. Acta B Atom Spectrosc.*, 2016, **125**, 103–110.
23 G. Cristoforetti, A. De Giacomo, M. Dell'Aglio, S. Legnaioli, E. Tognoni, V. Palleschi and N. Omenetto, *Spectrochim. Acta B Atom Spectrosc.*, 2010, **65**, 86–95.
24 H. R. Griem, *Principles of Plasma Spectroscopy*, 2005.
25 S. Sahal-Bréchot, M. S. Dimitrijević, N. Moreau and N. B. Nessib, *Adv. Space Res.*, 2014, **54**, 1148–1151.
26 A. M. Popov, T. F. Akhmetzhanov, T. A. Labutin, S. M. Zaytsev, N. B. Zorov and N. V. Chekalin, *Spectrochim. Acta B Atom Spectrosc.*, 2016, **125**, 43–51.
27 S. Djeniže, V. Milosavljević and A. Srećković, *J. Quant. Spectrosc. Radiat. Transf.*, 1998, **59**, 71–75.

28 N. Konjevic and W. Wiese, *J. Phys. Chem. Ref. Data*, 1976, **5**, 259–308.
29 N. a. L. A. a. F. J. R. a. W. W. L. Konjevic, *J. Phys. Chem. Ref. Data*, 2002, **31**, 819–927.
30 N. B. Nessib, *N. Astron. Rev.*, 2009, **53**, 255–258.
31 R. J. Schalkoff, *Artificial Neural Networks*, McGraw-Hill Higher Education, 1997.
32 É. Renault, S. Boumerdassi and P. Mühlethaler, *Machine Learning for Networking: Third International Conference, MLN 2020, Paris, France, November 24–26, 2020, Revised Selected Papers*, Springer Nature, 2021.
33 B. Yegnanarayana, *Artificial Neural Networks*, PHI Learning Pvt. Ltd., 2009.
34 S. Augst, D. Strickland, D. D. Meyerhofer, S.-L. Chin and J. H. Eberly, *Phys. Rev. Lett.*, 1989, **63**, 2212.
35 K. Jungwirth, A. Cejnarova, L. Juha, B. Kralikova, J. Krasa, E. Krousky, P. Krupickova, L. Laska, K. Masek and T. Mocek, *Phys. Plasmas*, 2001, **8**, 2495–2501.
36 A. a. R. Y. a. R. J. Kramida, *et al.*, *NIST Atomic Spectra Database (ver. 5.2)*, 2014.
37 M. Civiš, M. Ferus, A. Knížek, P. Kubelík, M. Kamas, P. Španěl, K. Dryahina, V. Shestivska, L. Juha and P. Skřehot, *Phys. Chem. Chem. Phys.*, 2016, **18**, 27317–27325.
38 R. R. Mahajan, S. A. Ehgamberdiev and S. Naik, *Planet. Space Sci.*, 2021, **207**, 105334.
39 J. Crabb and E. Anders, *Geochim. Cosmochim. Acta*, 1981, **45**, 2443–2464.
40 U. Ott, *Rev. Mineral. Geochem.*, 2002, **47**, 71–100.
41 L. Schultz and L. Franke, *Meteorit. Planet. Sci.*, 2004, **39**, 1889–1890.
42 U. Ott, T. D. Swindle and S. P. Schwenzer, in *Volatiles in the Martian Crust*, Elsevier, 2019, pp. 35–70.
43 I. MathWorks, *MATLAB: the Language of Technical Computing. Desktop Tools and Development Environment, Version 7, MathWorks*, 2005.
44 H. Demuth, M. Beale and M. Hagan, *For Use with MATLAB*, The MathWorks Inc, 1992, 2000.
45 I. B. Gornushkin, T. Völker and A. Y. Kazakov, *Spectrochim. Acta B Atom Spectrosc.*, 2018, **147**, 149–163.
46 D. Bulajic, M. Corsi, G. Cristoforetti, S. Legnaioli, V. Palleschi, A. Salvetti and E. Tognoni, *Spectrochim. Acta B Atom Spectrosc.*, 2002, **57**, 339–353.
47 F. Bredice, F. Borges, H. Sobral, M. Villagran-Muniz, H. O. Di Rocco, G. Cristoforetti, S. Legnaioli, V. Palleschi, L. Pardini and A. Salvetti, *Spectrochim. Acta B Atom Spectrosc.*, 2006, **61**, 1294–1303.
48 M. Burger, M. Skočić and S. Bukvić, *Spectrochim. Acta B Atom Spectrosc.*, 2014, **101**, 51–56.
49 L. Sun and H. Yu, *Talanta*, 2009, **79**, 388–395.
50 *Vienna Atomic Line Database (VALD)*, 2022. **https://vald.astro.uu.se/~vald/php/vald.php?docpage=about_vald.html**, accessed: 2022-01-20.
51 P. A. Loboda, *et al.*, *Atomic Database Spectr-W3 for Plasma Spectroscopy and other Applications*, 2022, **https://vald.astro.uu.se/~vald/php/vald.php?docpage=about_vald.html**, accessed: 2022-01-20.
52 *Tip Topbase*, 2022, **https://tiptopbase.obspm.fr/**, accessed: 2022-01-20.
53 *CHIANTI, An Atomic Database for Spectroscopic Diagnostics of Astrophysical Plasmas*, 2022, **https://www.chiantidatabase.org/**, accessed: 2022-01-20.
54 J. E. Hansen and W. Persson, *Phys. Scr.*, 1987, **36**, 602.
55 D. Luarte, A. K. Myakalwar, M. Velásquez, J. Álvarez, C. Sandoval, R. Fuentes, J. Yañez and D. Sbarbaro, *Anal. Methods*, 2021, **13**, 1181–1190.
56 J. Álvarez, M. Velásquez, A. K. Myakalwar, C. Sandoval, R. Fuentes, R. Castillo, D. Sbarbaro and J. Yáñez, *J. Anal. At. Spectrom.*, 2019, **34**, 2459–2468.
57 H. Saeidfirozeh and A. Shafiekhani, *Free Radic. Biol. Med.*, 2021, **177**, S88.
58 F. Ghaderi, A. H. Ghaderi, N. Ghaderi and B. Najafi, *Front. Chem.*, 2017, **5**, 99.
59 H. Busemann, H. Baur and R. Wieler, *Meteorit. Planet. Sci.*, 2000, **35**, 949–973.
60 G. R. Huss and R. S. Lewis, *Meteoritics*, 1994, **29**, 791–810.
61 F. a. B. A. Tholin, *J. Phys. D Appl. Phys.*, 2013, **46**, 319–330.
62 E. a. J. R. a. G. M. K. a. K. A. Mal, *J. Anal. At. Spectrom.*, 2019, **34**, 319–330.